Estimating propeller trailing-edge pressure using the BPM method

Richard Howell (1,2), Paul Croaker (1), Christopher Gargan-Shingles (1), Paul Dylejko (1) and Alex Skvortsov (1)

(1) Maritime Division, Defence Science and Technology Group, Melbourne, VIC 3207, Sydney, NSW 2015, Australia
(2) YTEK Pty Ltd, Level 1, 231 High St, Ashburton, VIC 3147, Australia

ABSTRACT

Vehicles moving through a fluid all suffer from unwanted noise and vibration from turbulent boundary layer excitation. Industries involved with designing planes, trains and automobiles have consequently invested heavily in its control. Large levels of noise and vibration can negatively impact on passenger and crew comfort as well as contributing to environmental noise. This paper details a novel approach for estimating the unsteady pressure at the trailing edge (TE) resulting from the turbulent boundary layer of a rotating propeller blade. This methodology is based on the semi-empirical method of Brooks, Pope and Marcolini known as the BPM method. Using a spanwise-strip implementation, the far-field TE noise is calculated for multiple points along the TE of the propeller surface of interest and at different positions of the propeller rotation. To provide quantitative validation of the numerical model, we present a comparison of estimated noise and trailing edge pressure characteristics with results obtained via experiment in the open literature. The noise estimates shown provide varying agreement using predictions of the flow field from the original empirical relationships and with those calculated using Reynolds Averaged Navier Stokes (RANS) CFD and the potential flow panel code XFOIL. The derived surface pressure characteristics are useful when evaluating the unsteady loading from the blade boundary layer flow.

1 INTRODUCTION

In the design of propellers, surface pressure characteristics are required when evaluating the unsteady loading and far-field noise from the blade turbulent boundary-layer (TBL). To avoid costly experiments, this data can be obtained through the use of high fidelity CFD e.g. Chen and MacGillivray (2014). To aid in the early design process a more rapid albeit less accurate evaluation of the radiated noise is warranted. These results can also be used to estimate the unsteady surface pressure; this is an example of an inverse technique e.g. Minniti et al. (2001) who inferred the inflow conditions from surface pressure measurements.

In this paper, we detail the development of a novel inverse trailing edge (TE) surface pressure model based on modifications to the BPM method (Brooks et al. 1989). Utilising experimental aeroacoustic measurements of the far-field sound pressure level (SPL) generated by TBL-TE interaction of different configurations of NACA0012 aerofoils in axial flow, Brooks, Pope and Marcolini developed a method to predict far-field TE noise using properties of the TBL. Assuming the noise from an individual spanwise segment is due to a compact point force radiating with a cardioid directivity, the force can be obtained from the BPM estimate of far-field SPL. Subsequently, this force can be converted to a pressure by dividing by the product of the spanwise and streamwise correlation lengths, a summary of the available correlation relationships can be found in Maxit et al. (2015). Herein we will apply the correlation model of Corcos (1964) as presented by Caiazzo et al. (2016).

Investigating published data for quantitative validation reveals many experimental studies that provide data on surface pressure and far-field SPL measurements for stationary symmetrical 2D aerofoils in axial flow e.g. Herr and Kamruzzaman (2013). However, we wish to validate a technique for rotating propellers and hence have selected the study of Rozenberg et al. (2010). In their study, aeroacoustic measurements were taken of a two bladed fan in air, the experimental set-up is shown at the top of Figure 1 with the global (X, Y, Z) axes. No additional axial free stream velocity was applied to the fan that was designed so that the sound generated was dominated by TE noise, i.e. the contributions to self-the noise from tip vortices, bluntness and turbulence ingestion were assumed to be negligible. The far-field noise was measured by a microphone at the end of the boom arm; the surface pressure was measured by the sensor layout shown at the bottom of Figure 1. These sensors were attached to the surface of the blades at the TE, one blade having a set at the mid-span and the other a set towards the tip.

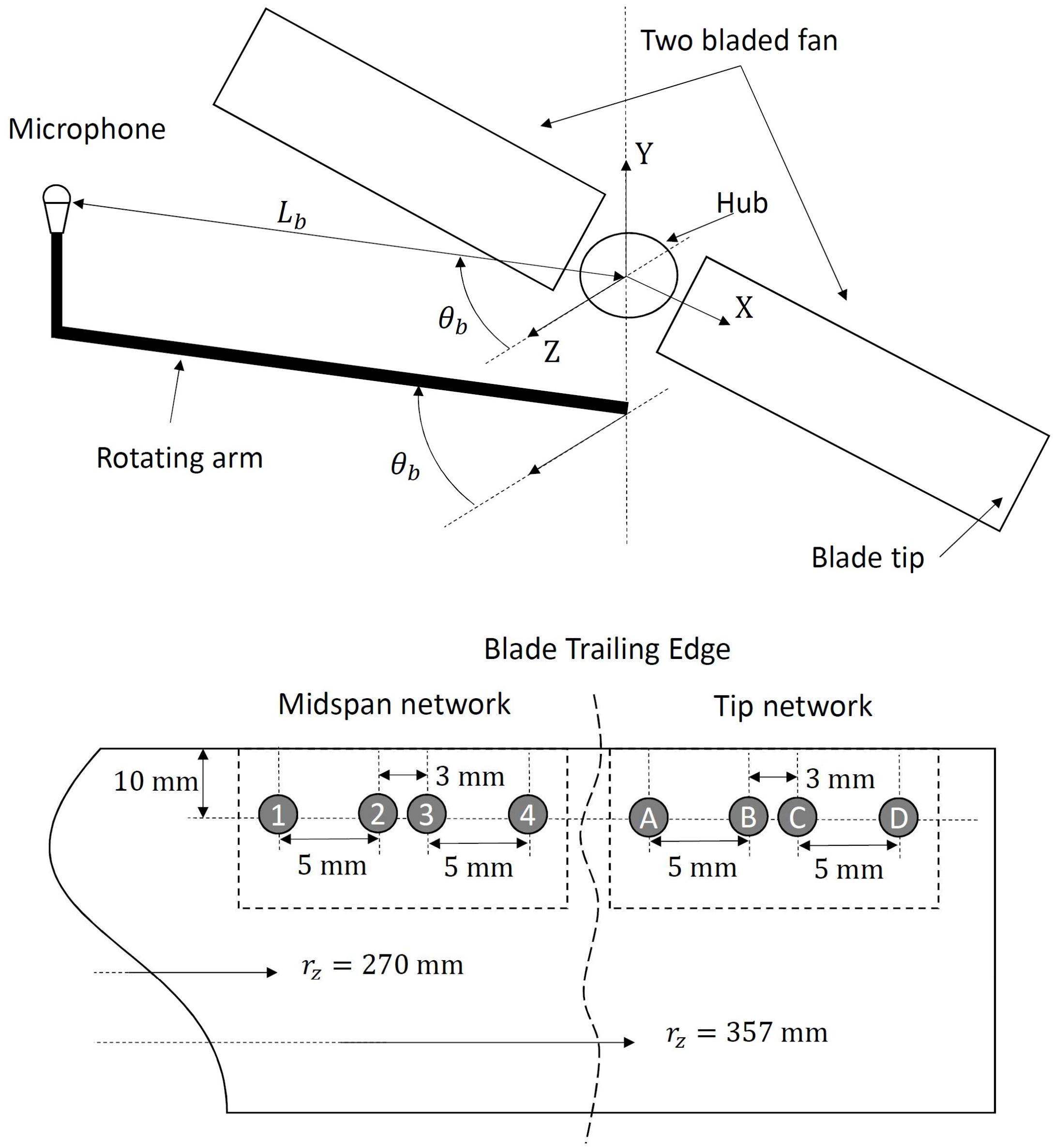

Figure 1: Top: Experimental set-up, Bottom: Surface pressure sensors (Rozenberg et al. 2010).

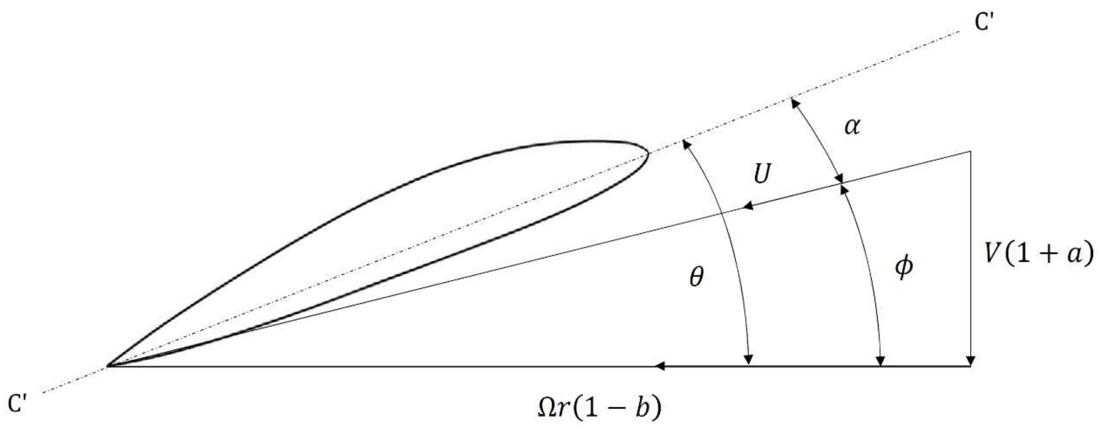

Figure 2: Classical Propeller Theory – vector diagram.

2 METHODS

2.1 Total Velocity & Effective Angle of Attack

The well-known BPM method of Brooks et al. (1989) estimates aerofoil TE far-field noise using empirical relationships based on the incident flow characteristics. The following shows how these can be obtained from classical propeller theory by representing the propeller as an actuator disk e.g. Houghton and Carpenter (2003). A single blade of chord length c and span L is discretised into N spanwise circumferential strips, giving a strip width of $\mathrm{d}L = L/N$. Owing to the rotation of the fan, each strip has a unique total velocity U and effective angle of attack α; these properties can be found by resolving the lift and velocity vectors shown in Figure 2. The value of U for each strip is composed of an axial velocity V and a tangential velocity Ωr_z, where r_z is a radial distance between 0 and L and Ω is the rotational frequency in rad/s. The value of α for each strip is equal to $\theta - \phi$ where θ is the geometric angle of attack ($\theta = 90 - \beta$ where β is the stagger angle) and ϕ is calculated from the following

$$\frac{V}{\Omega r_z} = \frac{(1-b)}{(1+a)} \tan\phi\,, \tag{2}$$

which is similar to an advance ratio that relates the forward speed to the rotational speed of the propeller that generates it. An iterative approach is used to calculate a and b that requires assuming the values of the lift to drag ratio (for the majority of aerofoils ≈ 50) and the lift curve slope or lift per degree (assuming thin plate theory ≈ 0.1 or $\approx 2\pi$ N lift per radian). An unknown input into Equation (2) is V that is equivalent to the axial flow speed through the fan and is also iterated for. To account for lower speeds towards the tip owing to loss of lift, a Prandtl Tip Loss function (PTL) is utilised e.g. Leishman (2006)

$$\mathrm{PTL}_z = \frac{2}{\pi}\cos^{-1}\left(e^{-\frac{B(L-r_z)}{2r_z\sin\phi}}\right), \tag{3}$$

that multiplies each value of a and b for every spanwise position r_z. The final flow information required are the boundary-layer thickness δ and displacement thickness δ^* that are estimated using U and α with the empirical relationships given by Brooks et al. (1989).

2.2 Far-field SPL

The BPM method estimates aerofoil TE far-field noise in one-third octave bands $\mathrm{SPL}_{1/3}$ (Pa^2). This noise can be generated from flow features originating from various different effects such as the skin friction on the pressure side or suction side and separation caused by increasing angle of attack or TE thickness. To calculate an average power-spectral density (PSD) of the far-field sound ϕ_{pp} $(\mathrm{Pa}^2/\mathrm{Hz})$, needed for the estimate of TE pressure outlined in the proceeding section, the following expression from Rozenberg et al. (2010) is used

$$\phi_{\mathrm{pp}} = \frac{1}{2\pi}\int_0^{2\pi} \phi_{\mathrm{pp}}^{\varphi}\, d\varphi = \frac{1}{I}\sum_{i=0}^{I} \phi_{\mathrm{pp}}^{i}. \tag{4}$$

The blades are rotated through $\varphi = 0{:}\,2\pi$ radians in I steps and the contributions from all the strips in all rotated positions are incoherently averaged. The value $\phi_{\mathrm{pp}}^{\varphi}$ at each boom angle is obtained by converting the BPM-derived far-field strip $\mathrm{SPL}_{1/3}$ values to PSD using the following expression

$$\phi_{\mathrm{pp}} = p_{\mathrm{o}}^2 10^{\mathrm{SPL}_{1/3}/10}/\delta f \qquad \text{as} \qquad \mathrm{SPL}_{1/3} = 10\log_{10}\left(\phi_{\mathrm{pp}}\,\delta f/p_{\mathrm{o}}^2\right), \tag{5a,b}$$

where p_{o} is the reference pressure that in air is 20μPa and δf is the width of the frequency band. An example calculation from Brooks et al. (1989) for the far-field noise generated by the flow over the suction side of the TE of an aerofoil is

$$\mathrm{SPL}_s = 10\log_{10}\left(\delta_s^* M^5 L \frac{D_h}{r^2}\right) + A\left(\frac{\mathrm{St}_s}{\mathrm{St}_1}\right) + (K_1 - 3)\,, \tag{6}$$

where r is the distance from the noise source to the observer, M is the Mach number and δ_s^* is the displacement thickness on the suction side. K_1 and A are semi-empirical functions, the latter is dependent upon the Strouhal Numbers St_s (suction side) and St_1 (M dependent). Setting $L = dL$ in Equation 6, $\mathrm{SPL}_{1/3}$ can be calculated for each strip. The directivity D_h is detailed in Brooks et al. (1989) as a cardioid: this is therefore dependent on the observer location that in this case is defined by the boom angle θ_b and boom length L_b shown in Figure 1. The value of D_h along with r^2 form a transfer function TF that relates a compact force to the far-field sound pressure e.g. see Ross (1976).

$$\mathrm{TF}^2 = k^2 D_h/(4\pi r)^2\,, \tag{7}$$

where k is the wave number ($= 2\pi f/c_0$, f is the frequency and c_0 is the speed of sound).

2.3 TE Pressure

To calculate the pressure at the TE, first the force must be calculated: the PSD of the force experienced at the TE ϕ_{ff} is related to ϕ_{pp} as

$$\phi_{\mathrm{ff}} = \phi_{\mathrm{pp}}/\mathrm{TF}^2, \tag{8}$$

where the units of ϕ_{ff} are N^2/Hz. The value of ϕ_{ff} is independent of the observer location. As noted in Section 1, ϕ_{ff} will be converted to a pressure by dividing by the product of the spanwise and streamwise correlation lengths. The correlation length techniques assume that the pressure fluctuations on a surface convect with the flow at a frequency dependent convection velocity U_c; this is the speed at which the turbulent eddies move in the boundary layer decelerated by wall friction and is typically in the range of $0.6U$ to $0.8U$ (Glegg and Devenport 2017). Corcos (1964) proposed an early form of a TBL surface-pressure model based on the Fourier transform of a curve fit of measured narrow-band pressure correlations, using simple exponentials to express correlation in the separate directions. Caiazzo et al. (2016) show that for a flow in the streamwise x direction relative to the foil, the spatial cross-spectral density for the Corcos model is equivalent to an ensemble of plane waves $e^{ik_c\xi_x}$ passing through spatial windows $e^{-|\xi_x|\alpha_\omega-|\xi_z|\beta_\omega}$. The terms ξ_x and ξ_z are distances along the propeller blade in respectively the streamwise direction x and spanwise direction z. $k_c = \omega/U_c$ is the convective wavenumber where $\omega = 2\pi f$. Using the notation of Caiazzo et al., the cross-spectral density of the fluid pressure underneath the TBL is denoted $\Psi_{pp}(\xi_x, \xi_z, \omega)$ and the PSD of the pressure $\phi(\omega)$ so that

$$\Psi_{pp}(\xi_x, \xi_z, \omega) = \phi(\omega) e^{ik_c\xi_x} e^{-|\xi_x|\alpha_c-|\xi_z|\beta_c}, \tag{9}$$

where the factor $e^{ik_c\xi_x}$ is required for the streamwise cross-spectrum to account for the effect of the mean convection of the flow. The coefficients are given by

$$\alpha_c = k_c\alpha_x \quad \text{and} \quad \beta_c = k_c\alpha_z\,, \tag{10a,b}$$

in which the longitudinal and lateral decay rates of the coherences are given by α_x and α_z respectively and their values are chosen to yield the best correlation with experiments; various values of these are given in the literature with the typical range for smooth rigid walls of α_x from 0.11 to 0.12 and α_z from 0.7 to 1.2. The force in Equation (8) can now be related to $\phi(\omega)$ by modifying Equation (9) into the following form

$$\phi_{\mathrm{ff}} = \phi(\omega)\, c dL \int_0^c \int_0^{dL} e^{ik_c\xi_x} e^{-|\xi_x|\alpha_c-|\xi_z|\beta_c}\, d\xi_x d\xi_z\,, \tag{11}$$

which can be rearranged to find $\phi(\omega)$ for a single strip. The double integration in Equation (11) is evaluated numerically using the trapezoidal rule with the integration points clustered towards the TE using the weighted polynomial method of Johnston and Elliott (2001).

3 RESULTS

3.1 Far-field SPL

Initial validation of the far-field SPL prediction (not shown here) was carried out with experimental results from Zajamsek et al. (2017). This work investigated a propeller with blades of uniform spanwise cross-section (NACA 0012) and chord length for geometric angles of attack of $\phi = 0^{\circ}$ and 10°; excellent agreement was found. In contrast, the propeller blades of Rozenberg et al. (2010) had varying spanwise cross-sections that were thin and of high curvature: as the BPM method is tuned to a NACA0012 foil, this will affect the empirical relationships for the BL and possibly the acoustic scattering. Also, although the spanwise chord length was relatively uniform ($c \approx$

0.12m) the value of ϕ was large causing a large effective angle of attack ($\alpha_{\text{TIP}} \approx 14^{\circ}$) for the rpm values studied, further affecting the empirical relationships for the BL. In Figure 3 the experimental data of Rozenberg et al. (2010) (discrete markers) are shown along with representative numerical results with $N = I = 10$ (solid lines) at four rpm values between 400rpm and 1000rpm. As predicted by Rozenberg et al. (2010) after calculation of the individual contributions to the far-field SPL the major constituents were found to be noise originating from the pressure and suction side and owing to the angle of attack. As predicted by Rozenberg et al. the tip vortex noise and bluntness noise were found to be small; they explained that the high value of α leads to a) flow separation that stops the formation of TE vortices that cause bluntness noise and b) the tip vortex to detach from the blade tip without interacting with the TE.

Overall, prediction of the SPL trend with frequency is poor owing to the effects noted above of curvature and high α, quantitative accuracy error as much as 10 dB around 1kHz. For such cases, it may therefore be more appropriate to use a semi-empirical model that is based on a prediction of surface pressure to calculate far-field sound e.g. Amiet (1976). However, predictions of the far-field SPL produced at 600rpm using flow data provided by alternate methods are shown in Figure 4 to determine whether improvements could be made to the results; therefore also plotted are the experimental data and the numerical model prediction of Figure 3 (red markers and red line respectively, the latter labelled PT for Propeller Theory). The magenta and black lines are predictions from a method developed by Doolan et al. (2019) that incorporates XFOIL (Drela 1989): the magenta line uses XFOIL to solely predict U and α, the BL properties being obtained from the BPM empirical relations. The black line uses XFOIL to predict the BL properties as well. The blue line is an 'Open Air' (OA) prediction (assume uniform axial flow across the span of the blades) and the blue line with circles is a RANS CFD prediction using the method detailed in Petterson et al. (2018). It can be seen in Figure 4 that surprisingly the OA prediction gives the best overall comparison, the effect of the blade design is perhaps to create a uniform axial flow across the span. Above 400Hz the predictions from RANS CFD are in excellent agreement with experiment, maximum error in general reduced to 3 dB. However, below 400Hz the RANS CFD under predicts the SPL: the RANS CFD predicts values of $\alpha \gg 12.5^{\circ}$ along the span so that the directivity is changed in the BPM method from a cardioid to a translating dipole for which the noise in this frequency range is not generated. The XFOIL+BPM method is of similar quality to that of the OA method whereas the full XFOIL method did not perform well: the latter result was attributed to an over prediction of the axial flow velocity as estimates of BL properties were of a similar magnitude to those predicted by the RANS CFD. The aerofoil geometry used in XFOIL was not that of the experiment as the aerofoil camber was too great to achieve a converged result: instead, for XFOIL+BPM a NACA 6409 profile was selected as it provided the main features of the actual blade cross section (thin and high curvature); for the XFOIL only case a NACA 0021 was used as this gave the best result from the profiles for which a solution could be obtained.

3.2 Spanwise Coherence & Wall Pressure PSD

The layout of the surface pressure sensors are shown in the bottom of Figure 1: those of interest are 1-4 of the midspan network and A-D in the tip network, sensors 1 and A of each set being the furthest from the blade tip/closest to the blade hub. In Figure 5, the experimental spanwise coherence values for the mid-span and tip are shown (discrete markers) for the same case as Figure 4 at 600rpm. Corcos (1964) formulated the following semi-empirical relation for spanwise coherence (denoted γ^2)

$$\gamma^2 = e^{-\frac{2\omega}{b_c U_c}\xi_z}, \tag{12}$$

where b_c is an empirical constant between 1.2 and 2 (Rozenberg et al. 2010). In Figure 5 we therefore also plot (as continuous lines) the predictions of Equation (12) from OA. For the example values chosen of $U_c = 0.7U$ and $b_c = 1.4$ the model predictions give closer agreement to the experiment for the tip set and at the root end of each set, though this may differ if these values are varied. In Figure 6 experimental values of wall-pressure PSD are plotted for the same case as Figure 4 at 600rpm. Experimental results shown are the maximum and minimum trends found at the midspan and tip sensor arrays. Using Equation (11) numerical predictions are also plotted in Figure 6 from OA (blue lines) and RANS CFD (blue lines with circles). In both cases it was found that varying the decay rates of α_x and α_z in the specified ranges noted in Section 2.3 had an insignificant effect on the numerical results. Although OA gave a reasonable overall SPL prediction, it was found that the individual-strip wall-pressure PSD values showed large variation between adjacent strips because of the poor prediction of δ^* at these high values of α. As such the lines were plotted using the force averaged over all strips calculated using Equation (8). However, this was not the case for the RANS CFD data where the prediction of δ^* was much improved and hence wall-pressure PSD varied gradually from strip to strip. Figure 6 shows that the RANS CFD results give better predictions: closer agreement is again found for the tip set and furthermore the prediction is better at higher frequencies. It is well known that the Corcos model has a lower accuracy at low frequencies, for example see Karimi et al. (2019); this is because the Corcos model over-estimates the low wavenumber, low frequency components (Caiazzo et al. 2016). The RANS CFD wall pressure PSD predictions demonstrate that the method of using the BPM model as an inverse method is viable and it is hoped would be more accurate using the XFOIL method as well for rapid predictions for propeller blades with lower values of α.

4 CONCLUSIONS

In this paper, we have detailed the development of a novel inverse trailing edge (TE) surface pressure model based on modifications to the BPM method (Brooks et al. 1989) to allow application to propellers. For quantitative validation purposes the experimental aeroacoustics study of a fan by Rozenberg et al. (2010) was selected for comparison. Varying quality of agreement was found between the experimental results for far-field SPL and the predictions that utilised the data provided by different flow methods. TE surface pressure predictions were less successful, the high effective angle of attack along the blades were beyond the accurate limits of classical propeller theory and XFOIL. However, reasonable quantitative agreement was found between the prediction using RANS CFD flow estimates and the experimental results. Future work will make additional validation of the wall-surface PSD predictions comparing to other surface pressure results in the open literature and utilise an improved correlation relationship at low wave numbers.

ACKNOWLEDGEMENTS

The authors would like to thank Alain Guedel at Cetiat and Stephane Moreau for kindly providing the 3D geometry of the fan from the study of Rozenberg et al. (2010).

REFERENCES

Amiet, R. K. (1976). "Noise due to turbulent flow past a trailing edge." *Journal of Sound and Vibration*, vol. 47(3), pp. 387-393. https://doi.org/10.1016/0022-460X(76)90948-2

Brooks, T. F., D. S. Pope and M. A. Marcolini (1989). *Airfoil self-noise and prediction*, NASA RP 1218.

Caiazzo, A., R. D'Amico and W. Desmet (2016). "A Generalized Corcos model for modelling turbulent boundary layer wall pressure fluctuations." *Journal of Sound and Vibration*, vol. 372, pp. 192-210. https://doi.org/10.1016/j.jsv.2016.02.036

Chen, L. and I. R. MacGillivray (2014). "Prediction of trailing-edge noise based on Reynolds-averaged Navier–Stokes solution." *AIAA Journal*, vol. 52(12), pp. 2673-2682. https://doi.org/10.2514/1.J052827

Corcos, G. (1964). "The structure of the turbulent pressure field in boundary-layer flows." *Journal of Fluid Mechanics*, vol. 18(3), pp. 353-378. https://doi.org/10.1017/S002211206400026X

Doolan, C., Y. Yauwenas and D. Moreau (2019). "Drone propeller noise under static and steady inflow conditions". *International Conference on Flow Induced Noise and Vibration Issues and Aspects*. https://doi.org/10.1007/978-3-030-64807-7_3

Drela, M. (1989). "XFOIL: An analysis and design system for low Reynolds number airfoils". *Low Reynolds number aerodynamics*. Springer, pp. 1-12. https://doi.org/10.1007/978-3-642-84010-4_1

Glegg, S. and W. Devenport (2017). *Aeroacoustics of low Mach number flows: fundamentals, analysis, and measurement*, Academic Press.

Herr, M. and M. Kamruzzaman (2013). "Benchmarking of Trailing-Edge Noise Computations---Outcome of the BANC-II Workshop". *19th AIAA/CEAS Aeroacoustics Conference*. https://doi.org/10.2514/6.2013-2123

Houghton, E. L. and P. W. Carpenter (2003). *Aerodynamics for engineering students*, Elsevier.

Johnston, P. R. and D. Elliott (2001). "A generalisation of Telles' method for evaluating weakly singular boundary element integrals." *Journal of Computational and Applied Mathematics*, vol. 131(1-2), pp. 223-241. https://doi.org/10.1016/S0377-0427(00)00273-9

Karimi, M., P. Croaker, A. Skvortsov, D. Moreau and N. Kessissoglou (2019). "Numerical prediction of turbulent boundary layer noise from a sharp-edged flat plate." *International Journal for Numerical Methods in Fluids*, vol. 90(10), pp. 522-543. https://doi.org/10.1002/fld.4733

Leishman, G. J. (2006). *Principles of helicopter aerodynamics*, Cambridge University Press.

Maxit, L., M. Berton, C. Audoly and D. Juvé (2015). "Discussion about different methods for introducing the turbulent boundary layer excitation in vibroacoustic models". *Flinovia-Flow Induced Noise and Vibration Issues and Aspects*. Springer, pp. 249-278. https://doi.org/10.1007/978-3-319-09713-8_12

Minniti, R., W. Blake and T. Mueller (2001). "Inferring propeller inflow and radiation from near-field response, Part 1: Analytic development." *AIAA Journal*, vol. 39(6), pp. 1030-1036. https://doi.org/10.2514/2.1443

Petterson, K., C. Fureby, M. Liefvendahl, D. Norrison and W. Sidebottom (2018). "LES of a full-scale self-propelled conventional submarine at±10 yaw". *32nd Symposium on Naval Hydrodynamics*.

Ross, D. (1976). *Mechanics of Underwater Noise*, Pergamon Press, New York.

Rozenberg, Y., M. Roger and S. Moreau (2010). "Rotating blade trailing-edge noise: Experimental validation of analytical model." *AIAA Journal*, vol. 48(5), pp. 951-962. https://doi.org/10.2514/1.43840

Zajamsek, B., C. J. Doolan, D. J. Moreau, J. Fischer and Z. Prime (2017). "Experimental investigation of trailing edge noise from stationary and rotating airfoils." *The Journal of the Acoustical Society of America*, vol. 141(5), pp. 3291-3301. https://doi.org/10.1121/1.4983295

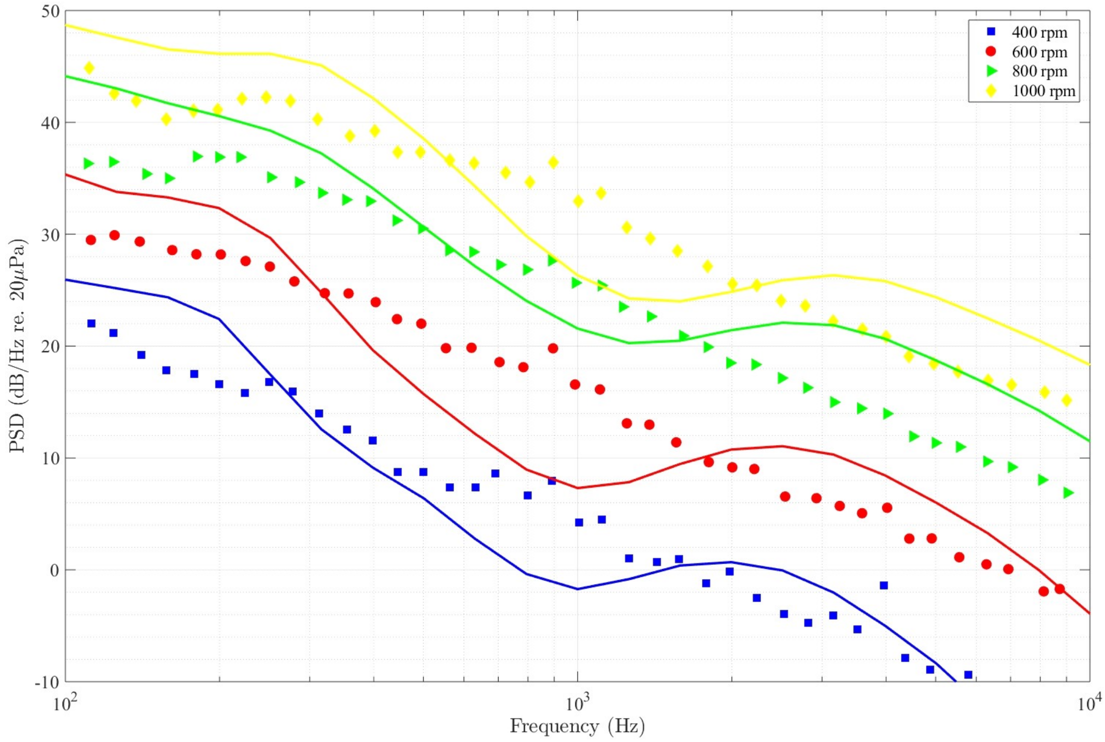

Figure 3: Self-noise spectra comparison with Rozenberg et al. (2010) ($\theta_b = 90^o, L_b = 1.7$m): Symbols – Experimental data, Solid lines – Predictions of method detailed in Section 2.

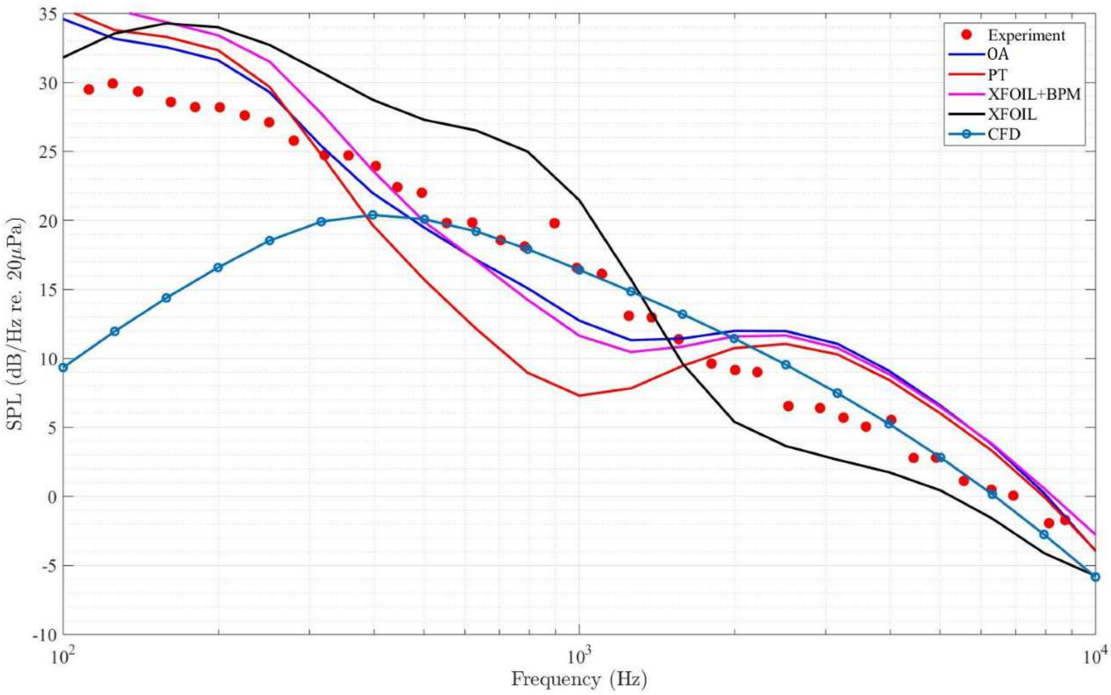

Figure 4: Self-noise spectra comparison with Rozenberg et al. (2010) at 600 rpm.

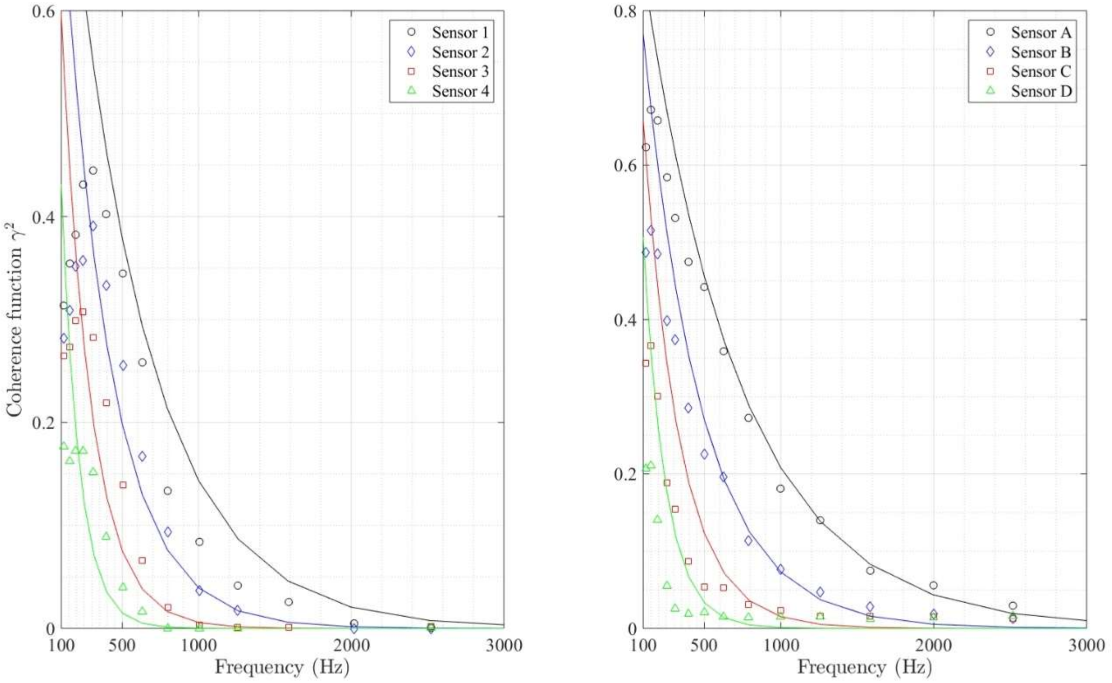

Figure 5: Comparison of coherence with Rozenberg et al. (2010) at 600 rpm – Left: mid section, Right: tip. Symbols – experimental data, Solid lines – OA predictions.

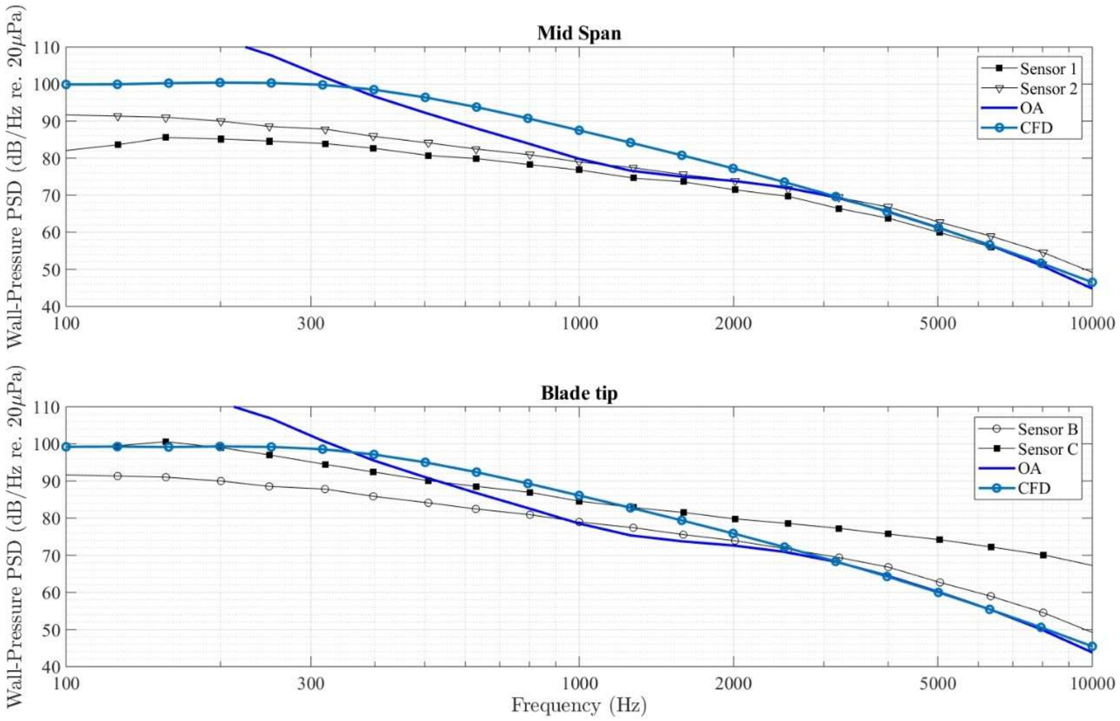

Figure 6: comparison of wall pressure PSD with Rozenberg et al. (2010) at 600 rpm – Top: midsection, Bottom: tip. Symbols – experimental data, Solid lines – Numerical predictions.